

Pincer Ligands

Access to and Reactivity of Fe⁰, Fe⁻¹, Fe^I, and Fe^{II} PC_{carbene}P Pincer Complexes

Qingyang Wang, Richard A. Manzano, Hendrik Tinnermann, Simon Sung, Baptiste Leforestier, Tobias Krämer* and Rowan D. Young*

Abstract: Despite their promising metal–ligand cooperative reactivity, PC_{carbene}P pincer ligands are rarely reported for first-row transition-metal centres. Using a dehydration methodology, we report access to an Fe⁰ PC_{carbene}P pincer complex (**1**) that proceeds via an isolated α -hydroxylalkyl hydrido complex (**3**). Reversible carbonyl migration to the carbene position in **1** is found to allow coordination chemistry and E–H bond addition (E = H, B, Cl) across the iron–carbene linkage, representing a unique mechanism for metal–ligand cooperativity. The PC_{carbene}P pincer ligand is also found to stabilize formal Fe^{II}, Fe^I, and Fe⁻¹ oxidation states, as demonstrated with synthesis and characterization of the complexes [II–X]–[BAr^F₂₀] (X = Br, I), **12**, and K[**13**]. Compound K[**13**] is found to be highly reactive, and abstracts hydrogen from a range of aliphatic C–H sources. Computational analysis by DFT suggests that the formal Fe^I and Fe⁻¹ complexes contain significant carbene radical character. The ability of the PC_{carbene}P ligand scaffold to partake in metal–ligand cooperativity and to support a range of iron oxidation states renders it as potentially useful in many catalytic applications.

Introduction

Tridentate meridional pincer ligands offer unique rigidity, selective activity and thermodynamic stability to transition metal centers.^[1] Such ligands have played an instrumental role in the development of transition metal catalysts capable of performing difficult bond transformations. PCP type pincers first reported by Shaw, containing a central metal–carbon bond flanked by two phosphorous donors, represent the earliest examples of pincer ligands, and have arguably contributed the most to the field.^[2]

Concurrent with the development of PCP pincer ligands has been a concerted drive towards the replacement of noble metal catalysts with base metal counterparts.^[3] This trend has

Zitierweise: *Angew. Chem. Int. Ed.* **2021**, *60*, 18168–18177
 Internationale Ausgabe: doi.org/10.1002/anie.202104130
 Deutsche Ausgabe: doi.org/10.1002/ange.202104130

been driven by economic and environmental factors, namely the high costs of noble metals and the toxicity involved with their extraction, handling and disposal. Indeed, the replacement of noble metals by base metals in catalysis is seen as an important area in developing green chemistry.^[3d]

To overcome the intrinsically lower activity of base metal catalysts, pincer ligands that exhibit metal–ligand cooperativity and high thermal stability have been developed.^[4] Such ligands can provide base metal complexes with comparable reactivity to many noble metal counterparts. In the realm of PCP pincer complexes, pincer ligands featuring central alkylidene donor atoms, termed PC_{carbene}P pincer ligands, have gained interest due to their unique metal–ligand cooperativity, their ability to stabilize a number of metal oxidation states, and the strong *trans* influence and effect of their central carbon donor.^[5]

Metal alkylidenes readily undergo 1,2-additions with a variety of strong bonds, thus C–H, Si–H, H–H and N–H bond activations have been reported in PC_{carbene}P complexes.^[6] However, PC_{carbene}P complexes have also demonstrated metal–ligand cooperation in [2+2] cycloadditions,^[7] frustrated Lewis pair chemistry,^[8] redox chemistry,^[9] catalytic deoxygenation and dechalcogenation chemistry,^[10] and ligand directed bond activation.^[11] Further, reports of bond activation and catalysis where the ligand acts only to support the metal fragment are also known.^[12]

Despite the many advantages of the PC_{carbene}P pincer framework, convenient access to complexes supported by these ligands has hindered development of the field. Although reports of Pt, Pd, Ir, Rh, Os and Ru are known (via double C–H activation of a proligand),^[13] access to base metal PC_{carbene}P pincer complexes remains challenging.^[14] Piers reported on Ni PC_{carbene}P complexes (Figure 1, **I**) generated from double electrophilic C–H activation of a proligand with [Ni^{II}Br₂] and strong base.^[6a,d,7d] This synthetic approach seems to be specific to group 10 complexes.


More recently, we have reported on access to PC_{carbene}P complexes via a dehydrative approach, which appears to be more facile and provides access to electron poor PC_{carbene}P complexes that are difficult to access via a double C–H activation approach. Access to a Co^I PC_{carbene}P pincer complex (Figure 1, **II**) was reported using this synthetic strategy.^[7a,15]

Milstein has reported a PCP ferraquinone system (Figure 1, **III**), accessed from oxidation of a ferrahydroquinone precursor.^[16] Unfortunately, Milstein could not obtain structural or spectroscopic metrics for the iron–carbene motif, preventing comparisons with data from previously reported

[*] Dr. Q. Wang, Dr. R. A. Manzano, Dr. H. Tinnermann, Dr. S. Sung, Prof. Dr. R. D. Young
 Department of Chemistry, National University of Singapore (Singapore)
 E-Mail: rowan.young@nus.edu.sg

Dr. B. Leforestier
 Department of Chemistry, University of Warwick (UK)

Dr. B. Leforestier, Dr. T. Krämer
 Department of Chemistry, Maynooth University (Ireland)
 E-Mail: tobias.kraemer@mu.ie

 Supporting information and the ORCID identification number(s) for the author(s) of this article can be found under:
<https://doi.org/10.1002/anie.202104130>

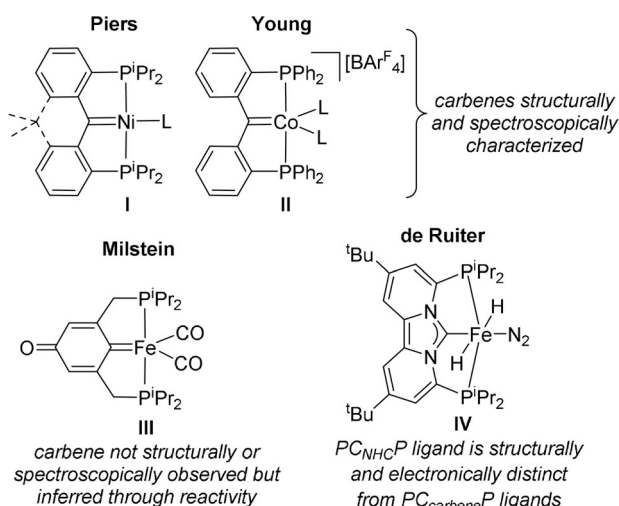


Figure 1. First-row transition metal $PC_{carbene}P$ complexes have been reported by Piers (I) and Young (II). Related iron examples of a ferriquinone (III) was reported by Milstein and a $PC_{NHC}P$ iron(II) complex (IV) was reported by de Ruiter.

Ni and Co systems, or with the Fe system in this report. It must also be noted that recently de Ruiter has reported a $PC_{NHC}P$ iron(II) pincer complex that was found to be an exceptional catalyst for H/D exchange reactions (Figure 1, IV).^[17] However, $PC_{NHC}P$ ligands are electronically and structurally different from $PC_{carbene}P$ systems in that they have very little metal-carbene double bond character, and rarely exhibit metal-ligand cooperativity.

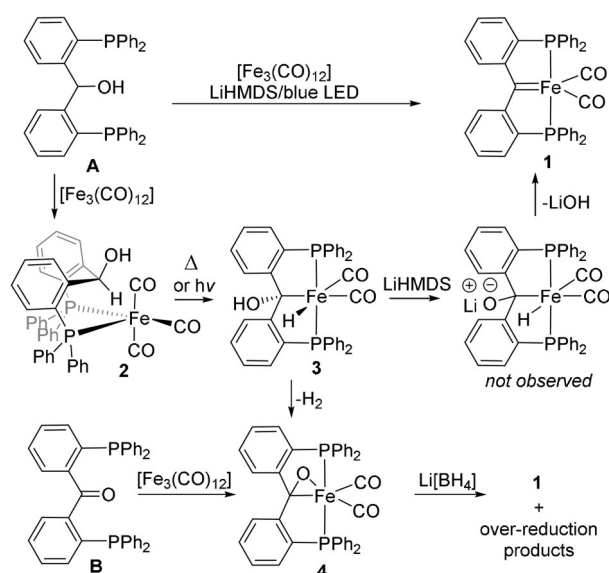
Thus, in an effort to expand the chemistry of base metal $PC_{carbene}P$ systems, we report here on the synthesis of an iron(0) $PC_{carbene}P$ complex (**1**) via proligand dehydration. We probe its electronic structure via reactivity with various reagents and DFT analysis, and explore its oxidation chemistry via generation of iron(II), iron(I) and iron(-I) $PC_{carbene}P$ pincer complexes.

Results and Discussion

Synthesis

Complex **1** was generated from proligand **A** in a two-step process that proceeded via complexes **2** and **3** (Scheme 1). Reaction of proligand **A** with $[Fe_3(CO)_{12}]$ afforded ready access to the chelate bisphosphino iron complex **2**, in a similar fashion to previously reported chemistry between triiron dodecacarbonyl and phosphino ligands.^[18]

A single crystal X-ray diffraction (SCXRD) study of **2** reveals that it adopts a pseudo trigonal bipyramidal (TBP) geometry in the solid state, with the two phosphine donors occupying axial and equatorial sites. Although the molecular structure of **2** exhibits a short methine-iron C-H-Fe distance {C-Fe = 3.702(3) Å, H-Fe = 2.946(3) Å}, the full valence electron count of iron renders any agostic interaction unlikely, although an electrostatic anagostic interaction remains feasible (Figure 2). Additionally, the C1-Fe1 distance of 3.702-



Scheme 1. Synthesis of $PC_{carbene}P$ iron complex **1** from $[Fe_3(CO)_{12}]$ and proligand **A**. Complex **1** is accessed through formation of complex **2** then via α -hydroxyalkyl complex **3**. Complex **1** can also be generated from the reduction of complex **4**.

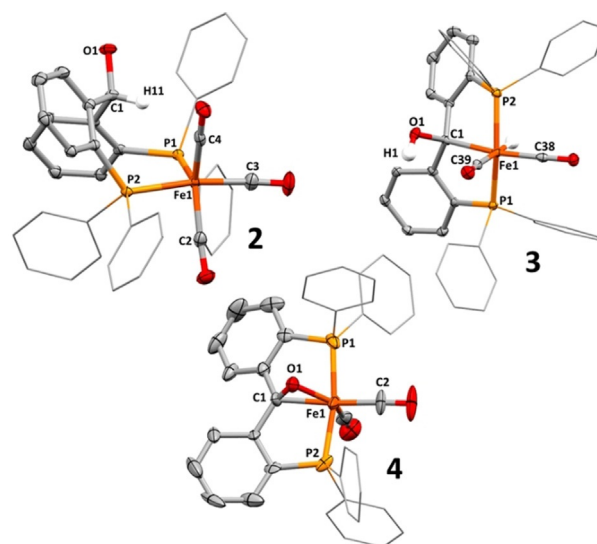


Figure 2. Molecular structures of compounds **2–4**. Hydrogen atoms (except H11 in **1** and H1 in **2**) omitted, thermal ellipsoids shown at 50%. H11 and H1 were located in the Fourier Difference map. Selected bond distances (Å) and angles (°): for **2**; Fe1-P1, 2.236(1); Fe1-C1, 3.702(3); P1-Fe1-P2, 99.9(3); for **3**; Fe1-P1, 2.166(1); Fe1-C1, 2.146(3); C1-O1, 1.467(3); P1-Fe1-P2, 158.9(1); C1-Fe1-C38, 166.9(1); for **4**; Fe1-P1, 2.186(5); Fe1-C1, 2.013(7); Fe1-O1, 1.887(7); C1-O1, 1.39(1); P1-Fe1-P2, 168.7(2); C2-Fe1-C1, 161.4(5).

(3) Å is well outside the sum of covalent radii of a Fe-H-C interaction ($\Sigma_{FeHHC} = 2.70$ Å).^[19]

Compound **2** provided a single broad ³¹P NMR resonance at $\delta_p = 57.4$ at room temperature, consistent with fluxional exchange between phosphine axial/equatorial sites, but the IR resonances due to carbonyl ligand stretching at 1983, 1916 and

1866 cm^{-1} are consistent with the retention of a TBP structure in solution.^[20]

Compound **2** could be converted directly to compound **1** upon irradiation with blue light in the presence of the non-nucleophilic base LiHMDS in 72% yield. However, when dissolved in THF in the absence of base, **2** underwent slow carbonyl loss and C-H activation^[21] at the central methine position to generate complex **3**. This process could be accelerated via heating at reflux or exposure to blue LED light. Compound **3** was structurally characterized as an α -hydroxyalkylhydrido iron(II) complex (Figure 2). Spectroscopic data support this connectivity, with compound **3** displaying a hydrido signal at $\delta_{\text{H}} = -7.76$ (t, $^2J_{\text{PH}} = 55.8$ Hz) and a hydroxyl signal at $\delta_{\text{H}} = 2.26$. Correlation spectroscopy revealed a ^{13}C resonance at $\delta_{\text{C}} = 106.2$ (t, $^2J_{\text{PC}} = 11.0$ Hz) arising from the central alkyl carbon donor atom. α -Hydroxyalkyl ligands are kinetically unstable but have previously been shown to be accessible from both alcohol and ketone precursors.^[22]

Overtime, compound **3** eliminates either hydrogen to generate compound **4** or water to generate the desired product, $\text{PC}_{\text{carbene}}\text{P}$ complex **1** (Scheme 1). It was observed that the presence of a strong, non-nucleophilic base (e.g. LiHMDS) promoted conversion to complex **1**, while protic conditions (e.g. in the presence of liberated water) generate a mixture of **4** and **1**. Notably, the molecular structure of **3** (Figure 2) indicates that the hydroxyl and hydrido groups are in an *anti* configuration, representing a barrier to elimination of water.

Significantly, **3** represents the characterization of an intermediate that we have postulated enroute to group 9 $\text{PC}_{\text{carbene}}\text{P}$ pincer complexes, but have never observed due to the fast elimination of water from group 9 cationic α -hydroxyalkyl hydride complexes.^[7a,b,11]

Compound **4** could be generated in a more direct manner via addition of the keto proligand **B** to $[\text{Fe}_3(\text{CO})_{12}]$ (Scheme 1). Compound **4** could be subsequently reduced with lithium borohydride to generate **1**, however, this also led to „over-reduction“ products (see below), so was not a convenient route to **1**.

SCXRD analysis of **1** showed two crystallographically independent molecules crystallising in a P_{21} spacegroup. The independent molecules adopt pseudo square pyramidal (**1-SQP**) and trigonal bipyramidal (**1-TBP**) structures with τ values of 0.24 and 0.49 respectively (Figure 3).^[23] Closely related PNP pincer complexes have been reported to adopt both TBP and SQP geometries by Chirik, and Krogh-Jespersen and Goldman.^[24] *In silico* geometry optimisation of **1** (see below) suggested that the SQP structure is slightly energetically preferred over TBP. An FTIR spectrum of **1** in benzene shows two CO stretching bands at 1953 and 1893 cm^{-1} respectively, suggesting either (i) that a single geometry (likely SQP) is adopted in solution, or (ii) that both forms of **1** have coincident CO stretching frequencies.^[24b]

In each of the geometries of **1**, the Fe–C bond distances to the PCP ligands are within statistical error of each other, with an average Fe–C bond distance of 1.914(7) Å supporting the assignment of **1** as a $\text{PC}_{\text{carbene}}\text{P}$ pincer complex. Further, the ^{13}C NMR spectrum of **1** reveals a low field signal at $\delta_{\text{C}} = 241.3$

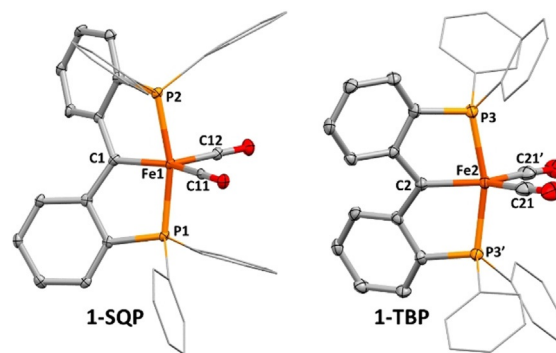


Figure 3. Molecular structures of the two crystallographic independent units of compound **1** with pseudo square pyramidal (**1-SQP**) and trigonal bipyramidal (**1-TBP**) geometries. Thermal ellipsoids shown at 50%. Selected bond distances (Å) and angles ($^\circ$): for **1-SQP**; Fe1–P1, 2.202(1); Fe1–P2, 2.188(1); Fe1–C1, 1.913(5); P1–Fe1–P2, 164.7(1); C1–Fe1–C11, 150.1(2), C1–Fe1–C12, 114.5(2); for **1-TBP**; Fe2–P3, 2.214(1); Fe2–C2, 1.914(6), P3–Fe1–P3', 163.2(1); C2–Fe1–C21, 133.7(2).

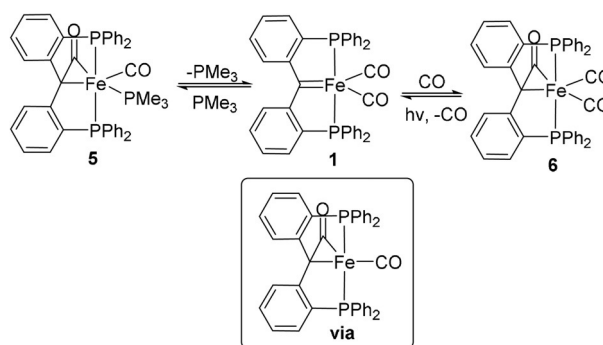
with significant coupling to the two phosphorus donor atoms (t, $^2J_{\text{CP}} = 30.1$ Hz).

In general, iron alkylidene complexes are kinetically unstable. However, chelate stabilized iron alkylidene complexes offer a unique opportunity to probe the character and reactivity of iron-carbene linkages similar to those in a range of intermediates of interest.^[14,26]

Reactivity Studies

The full valence shell configuration of compound **1** rendered it unreactive with weaker σ -donor L type ligands such as PPh_3 , dpmm and NEt_3 . However, compound **1** was found to be able to isomerise to accommodate PMe_3 and CO ligands to generate compounds **5** and **6** respectively (Scheme 2). Compounds **5** and **6** feature a η^2 -ketene donor formed by migration of a carbonyl ligand to the pincer carbene position.

In solution, compound **5** is in equilibrium with compound **1** ($K_{\text{eq}} \approx 0.25$). As such, compound **5** reforms compound **1** in the absence of excess free PMe_3 , hampering efforts to isolate pure samples of complex **5**. As the process of ligand loss was



Scheme 2. Reaction of **1** with excess PMe_3 to generate **5**, or excess CO to generate **6**.

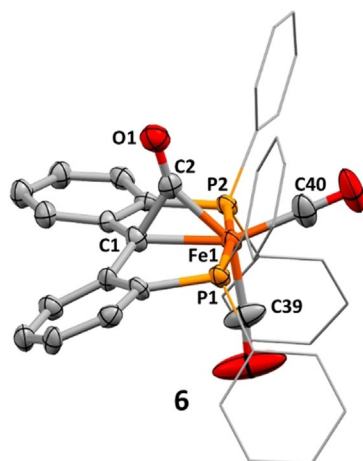


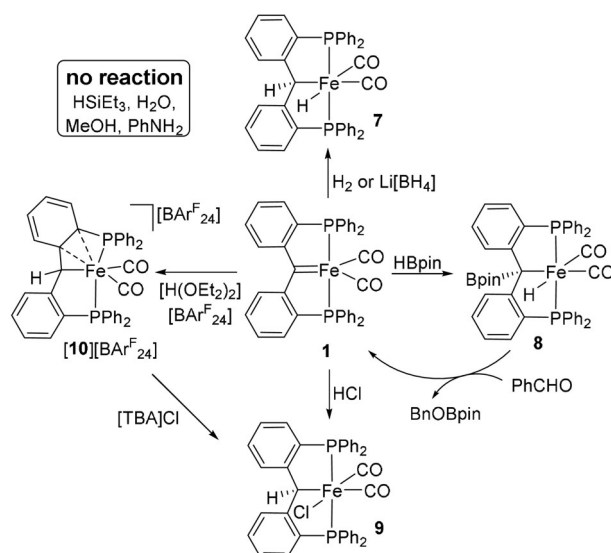
Figure 4. Molecular structure of compound **6**. Hydrogen atoms omitted, thermal ellipsoids shown at 50%. Selected bond distances (Å) and angles (°): Fe1-P1, 2.202(1); Fe1-C1, 2.096(2); Fe1-C2, 1.877(2); C1-C2, 1.512(3); C2-O1, 1.190(3); P1-Fe1-P2, 171.2(1); C39-Fe1-C40, 103.7(1); C1-Fe1-C40, 152.0(1); C1-Fe1-C39, 104.2(1).

found to have a very low barrier, compound **5** could only be characterized in situ in the presence of excess PMe_3 . In contrast, compound **6** (formed under an atmosphere of carbon monoxide) was found to be relatively thermally stable in solution and crystallisation at low temperature yielded crystals of X-ray diffraction quality (Figure 4).

The molecular structure of compound **6** reveals a pseudo trigonal pyramidal geometry, with an elongated Fe1–C1 distance of 2.096(2) [cf. 1.913(5) in **1**]. The bridging carbonyl's C–O bond length was also slightly elongated {1.190(3) Å} versus the terminal carbonyl ligand C–O bond lengths {C–O_{mean} = 1.120(5) Å}, indicative of more double bond character in the bridging C–O bond.

Although a molecular structure of **5** could not be obtained, similar spectroscopic data imply a congruent structure to **6**. For example, compound **5** features a low-field signal in its ^{13}C NMR spectrum corresponding to the bridging carbonyl at $\delta_{\text{C}} = 241.7$ (dt, $^2J_{\text{PC}} = 27.1, 17.2$ Hz). Compound **6** features a bridging carbonyl signal at $\delta_{\text{C}} = 242.1$, although it is too broad to resolve fine structure multiplicity. Additionally, both compounds **5** and **6** feature ketene stretching frequencies at 1685 cm^{-1} and 1700 cm^{-1} respectively. However, compound **5** features only a single terminal CO stretching band at 1894 cm^{-1} , while **6** features two bands at 2005 cm^{-1} and 1938 cm^{-1} . Although **6** was found to be largely thermally stable, with only minimal decomposition when heated to 80°C , it was found to be photosensitive and reverted to compound **1** in a matter of hours when irradiated in solution. Similar η^2 -ketene to $\text{PC}_{\text{carbene}}\text{P}$ conversions have been observed for complexes reported by Piers under thermally promoted conditions.^[26]

Given the success that analogous $\text{PC}_{\text{carbene}}\text{P}$ complexes have had in facilitating bond activation via metal-ligand cooperativity, we attempted to activate a number of hydrogen-element bonds (Scheme 3). Compound **1** was found to react with hydrogen (4 atm) at room temperature with



Scheme 3. Metal-ligand cooperativity in **1** allowed the activation of H_2 , HBpin and HCl to generate compounds **7**, **8** and **9** respectively. Compound **9** could also be accessed by sequential addition of H^+ (generating $[10][\text{BARF}_{24}]$) then Cl^- .

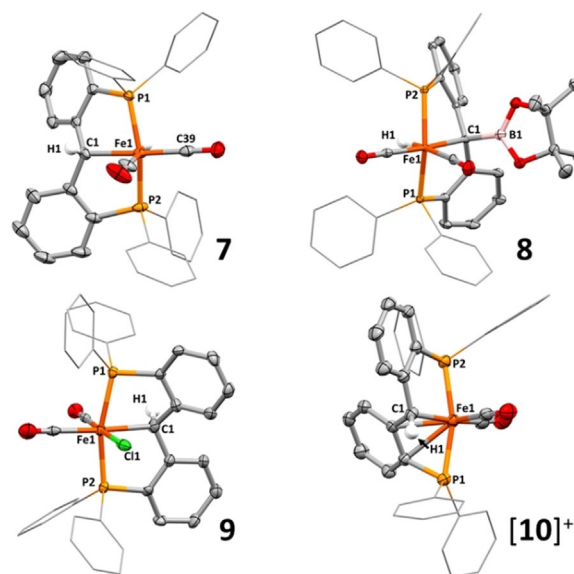


Figure 5. Molecular structures of compounds **7**–**[10]**⁺. Hydrogen atoms (except H1 in **7**–**[10]**⁺) and anion (for **[10]**⁺) omitted, thermal ellipsoids shown at 50%. Selected bond distances (Å) and angles (°): for **7**; Fe1-P1, 2.182(1); Fe1-C1, 2.126(2); P1-Fe1-P2, 158.3(1); for **8**; Fe1-P1, 2.172(1); Fe1-C1, 2.190(2); C1-B1, 1.572(3); P1-Fe1-P2, 154.8(1); for **9**; Fe1-P1, 2.251(2); Fe1-C1, 2.129(6); Fe1-Cl1, 2.298(4); P1-Fe1-P2, 164.3(1); C1-Fe1-Cl1, 87.7(2); for **[10]**⁺; Fe1-P1, 2.198(1); Fe-P2, 2.231(1); Fe1-C1, 2.068(3); P1-Fe1-P2, 163.9(1).

complete conversion of **1** to the iron(II) hydride **7** observed over 12 hours (Figure 5). Compound **7** was also identified as an „over-reaction“ product in the reduction of compound **4** to **1** with $\text{Li}[\text{BH}_4]$ described above (Scheme 1), and could be obtained in low yield from the direct reaction of $\{\text{CH}_2((\text{C}_6\text{H}_4)\text{PPh}_2)_2\}$ with $[\text{Fe}_3(\text{CO})_{12}]$ under blue light irradiation.

The hydroborane HBpin was found to add across the metal-carbene linkage in **1** to generate the $\text{PC}_{\text{sp}^3}\text{P}$ pincer **8** with the boryl group directed to the pincer carbon and the hydride to the iron centre. Reaction of **8** with PhCHO at 100 °C overnight regenerated **1** along with BnOBpin, forming the basis of a potential catalytic cycle that utilizes ligand cooperativity. Interestingly, the molecular structures of both **7** and **8** reveal an *anti* configuration between the iron hydride and central pincer substituents (H or Bpin). Given that it would be expected that concerted addition of either H_2 or HBpin to **1** would result in a *syn* configuration, we carried out a DFT study to explore possible mechanistic pathways for these activations.

The pathway for H_2 addition to **1** is shown in Scheme 4 (see ESI for more details and Figure S67 for a pathway of HBpin addition). Initial isomerisation of **1** via migratory insertion of a carbonyl into the pincer $\text{Fe}=\text{C}$ bond ($\Delta G^\ddagger = 11.0 \text{ kcal mol}^{-1}$) enables side-on coordination of H_2 to the Fe centre (**Int_{II}**, cf. formation of **5** and **6**). Interestingly, all attempts to locate a transition state corresponding to concerted 1,2-addition of H_2 across the $\text{Fe}=\text{C}$ bond were unsuccessful. Instead, cleavage of the H_2 bond from **Int_{II}** proceeds through direct proton transfer to the pincer alkyl carbon (**TS_{II}**, $\Delta G^\ddagger = 23.7 \text{ kcal mol}^{-1}$), furnishing the *syn*-isomer of **7** ($\Delta G = -11.9 \text{ kcal mol}^{-1}$). The alternative stepwise mechanism,^[27] that is, oxidative addition of H_2 followed by proton transfer onto the pincer carbon atom, was found to be kinetically less favourable (see ESI). Subsequent C-H reductive elimination ($\Delta G^\ddagger = 18.6 \text{ kcal mol}^{-1}$) generates **Int_{III}** ($\Delta G = -4.8 \text{ kcal mol}^{-1}$). Rearrangement towards the *anti*-isomer can now occur via pivoting of the CH_2 unit, with a small activation barrier ($\Delta G^\ddagger = 5.6 \text{ kcal mol}^{-1}$) and an $\eta^2\text{-H}_2$ agostic intermediate (**Int_{IV}**). This step positions the two methylene hydrogens onto opposite sides of each other, and subsequent C-H oxidative addition (**TS_V**) yields the experimentally observed *anti*-isomer of **7** as the thermodynamic product ($\Delta G = -14.5 \text{ kcal mol}^{-1}$).

The pathway for addition of pinacolborane follows a similar mechanism (see ESI, Figure S67). In this case proton transfer and concomitant boryl migration to the iron centre is again energetically favourable, while concerted 1,2-addition of the B-H bond across the $\text{Fe}=\text{C}$ bond is found to be considerably higher in energy. An alternative frustrated Lewis pair (FLP) type reaction pathway that exploited the ambi-

philic nature of the carbene position was explored for the activation of both H_2 and HBpin but discarded due to energetically inaccessible intermediates (see ESI, Figure S72).

Notably, **Int_I** (Scheme 4) appears to be requisite for the formation of compounds **5–8**. Indeed, a competent reaction pathway for the formation of **6** was computationally mapped via **Int_I** (see ESI, Figure S70), and the stability of compounds **5** and **6** relative to **Int_{II}** (Scheme 4) corresponds to their calculated free energies with respect to **1** (see ESI, Figure S71). The ability of **1** to isomerize to form a 16 valence e^- metal complex is key to its reactivity. Although $\text{PC}_{\text{carbene}}\text{P}$ pincers have been observed to sequester hydride ligands to enhance reactivity at a metal centre,^[6c] this example is unique in that the migration of CO to the carbene position still allows bond addition across the metal-carbon linkage (i.e. metal-ligand cooperativity, **TS_{II}**, Scheme 4).

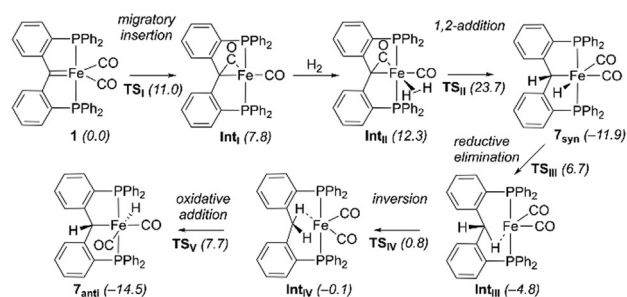
When compound **1** was reacted with HCl, the *anti* isomer of compound **9** was predominantly generated. As opposed to the addition of H_2 and HBpin, the addition of HCl might be expected to occur in a stepwise fashion, where the thermodynamic product would be more kinetically accessible. Indeed, compound **9** could also be generated via addition of $[\text{H}(\text{OEt}_2)_2][\text{BAR}^{\text{F}}_{24}]$ $\{[\text{BAR}^{\text{F}}_{24}] = \text{tetrakis}(3,5\text{-bis}(\text{trifluoromethyl})\text{phenyl})\text{borate}\}$ to **1** to generate compound **[10][BAR^F₂₄]**, followed by the addition of nucleophilic chloride in the form of tetrabutylammonium chloride (TBA-Cl). In compound **[10][BAR^F₂₄]** the pincer backbone contorts to allow η^2 -coordination of a pincer phenylene to fulfil the iron's effective atomic number (EAN) requirements. Addition of chloride to **[10][BAR^F₂₄]** to generate **9** is likely facile due to the re-aromatization of the phenylene ring after displacement from the iron centre.

Protonation of the carbenic site stands in stark contrast to isoelectronic d^8 group 9 and 10 complexes (found to have poorly nucleophilic carbene sites), and more closely mirrors the reactivity observed in zero valent group 10 $\text{PC}_{\text{carbene}}\text{P}$ complexes. However, the carbene linkage in compound **1** appears to be much more stable than those reported for $d^{10}\text{PC}_{\text{carbene}}\text{P}$ complexes. For example, in contrast to Ni and Pd $\text{PC}_{\text{carbene}}\text{P}$ pincer complexes reported by Piers and Iluc,^[6] compound **1** was found to be stable in the presence of water, alcohol, amine and hydrosilane.

Redox Behaviour

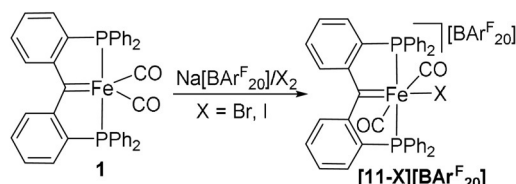
A unique feature of iron pincer chemistry is the ability of iron to access a wide variety of oxidation states. To complement this, $\text{PC}_{\text{carbene}}\text{P}$ pincer ligands have been shown to allow ligand centred redox chemistry that offers an extra dimension to the redox chemistry of **1**. To that end, we explored the ability of the $\text{PC}_{\text{carbene}}\text{P}$ pincer framework to support multiple (formal) oxidation states of iron.

Addition of either iodine or bromine to **1** with an equivalent of $\text{Na}[\text{BAR}^{\text{F}}_{20}]$ $\{[\text{BAR}^{\text{F}}_{20}] = \text{tetrakis}(\text{pentafluorophenyl})\text{borate}\}$ led to formation of the iron(II) $\text{PC}_{\text{carbene}}\text{P}$ pincer complexes **[11-X][BAR^F₂₀]** (X = Br, I) (Scheme 5). The products **[11-Br][BAR^F₂₀]** and **[11-I][BAR^F₂₀]** could readily be



Scheme 4. DFT-calculated reaction pathway for activation of H_2 by **1**. Free Energies (ΔG_{298} in kcal mol^{-1}) are given in brackets, see SI for details.

Two electron oxidation



Scheme 5. Reaction of **1** with Na[BAr^F₂₀] and X₂ (X = Br, I) yields complexes [11-X][BAr^F₂₀] in 82% (X = Br) and 81% (X = I).

isolated in 82% and 81% yields, respectively. Molecular structures of [11-X][BAr^F₂₀] (X = Br, I) reveal both complexes feature the halido ligand *trans* to the carbene donor (Figure 6). Additionally, very short Fe–C bond distances are observed for the carbene donor atoms {Fe1–C1 in [11-Br]⁺ = 1.879(3) Å, in [11-I]⁺ = 1.907(4) Å}.

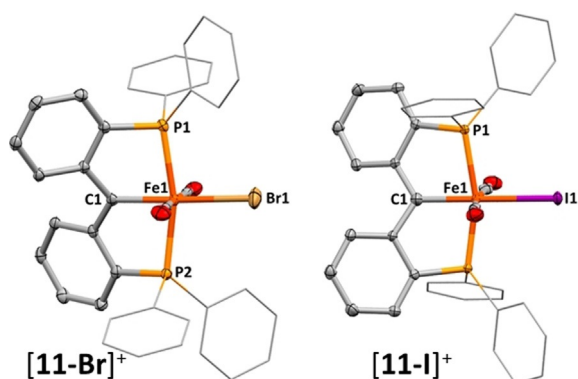
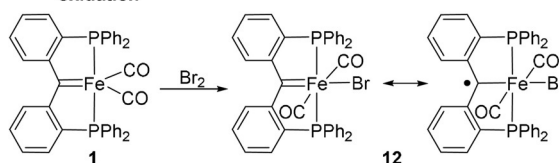


Figure 6. Molecular structures of compounds [11-X]⁺ (X = Br, I). Hydrogen atoms and anions omitted, thermal ellipsoids shown at 50%. Selected bond distances (Å) and angles (°): for [11-Br]⁺; Fe1–P1, 2.269(1); Fe1–C1, 1.879(3); Fe1–Br1, 2.464(1); P1–Fe1–P2, 165.6(1); C1–Fe1–Br1, 178.6(1); for [11-I]⁺; Fe1–P1, 2.261(1); Fe1–C1, 1.907(4); Fe1–I1, 2.618(1); P1–Fe1–P1', 163.6(1); C1–Fe1–I1, 180.0(1).

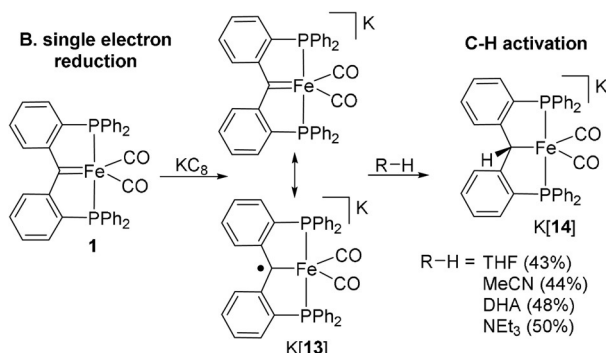
Both iron(II) carbene complexes display very low field carbene atom ¹³C NMR resonances at δ_C = 350.4 for [11-Br]⁺ and δ_C = 350.9 (t, ²J_{CP} = 8.5 Hz) for [11-I]⁺. These are much more downfield than the carbene signal of **1** (δ_C = 241.3) as would be expected for carbene donors with a higher degree of Fischer carbene character. FTIR analysis also revealed the electron poor character of the iron(II) PC_{carbene}P complexes. Compound [11-Br]⁺ displays a strong CO stretching band at 2043 cm⁻¹, and [11-I]⁺ has a similar CO stretching frequency at 2035 cm⁻¹.

Next, a single electron oxidation of **1** was attempted. A common approach for the single electron oxidation of group 10 PC_{carbene}P pincer complexes is the addition of elemental halogen as an oxidant. In the case of **1**, addition of iodine led to the formation of [11-I][I₃], featuring a triiodide counteranion. However, addition of elemental bromine to **1** did induce single electron oxidation to generate the formal iron(I) bromide species **12** (Scheme 6A) isolated in 65% yield. Compound **12** could also be generated by the reduction of [11-Br][BAr^F₂₀] with cobaltocene.

A. single electron oxidation



B. single electron reduction



Scheme 6. A) Single electron oxidation of **1** with Br₂ generates **12** in 65% yield. B) Single electron reduction of **1** with KC₈ generates K[13] in 57% isolated yield. Further reaction of K[13] with hydrogen atom sources generates K[14] via a HAT C-H activation reaction.

The formation of **12** likely occurs via a comproportionation between **1** and in situ generated [11-Br]Br. Indeed, a control reaction between **1**, [11-Br][BAr^F₂₀] and [TBA]Br also led to the formation of **12**. In the presence of Na[BAr^F₂₀], free bromide is sequestered faster than the comproportionation reaction occurs, allowing the formation [11-Br][BAr^F₂₀] as opposed to **12**.

The formation of compound **12** was apparent by the appearance of a new IR signal in the solution FTIR spectrum of the reaction mixture at 1968 cm⁻¹. Additionally, the formation of a paramagnetic species observable by ¹H NMR and EPR spectroscopy, also provided additional spectroscopic evidence for the existence of **12**.

Crystals of **12** (formed from a concentrated solution in benzene) allowed structural determination of **12** through a single crystal X-ray diffraction study (Figure 7). Compound **12** adopts an octahedral geometry with the bromide ligand occupying the site *trans* to the pincer carbene donor atom. Complex **12** displays a much longer Fe–C bond distance to the carbene ligand {Fe1–C1 = 1.998(2) Å} than either **1** or [11-X][BAr^F₂₀] (X = Br, I), however, a much shorter Fe–C bond distance as compared to compounds featuring PC_{alkyl}P pincer ligands, that is, compounds **3**, **7**, **8** and **9** {Fe1–C1 = 2.126(2) to 2.190(2) Å}. This can be interpreted as a lower degree of double bond character (*cf* [11-X]⁺) arising from a radical carbene nature.^[28] Indeed, solid-state EPR revealed a signal at g_{iso} = 2.0149, typical of a radical carbene species.^[9]

Single electron reduction of **1** was attempted to generate the formally iron(-I) species K[13] (Scheme 6B). Treating a sample of **1** dissolved in benzene with an equivalent of potassium graphite (KC₈) led to an immediate colour change from dark green to brown. The filtered solution quickly deposited K[13] as a deep purple microcrystalline precipitate in 57% yield that could not be redissolved in arene solvent.

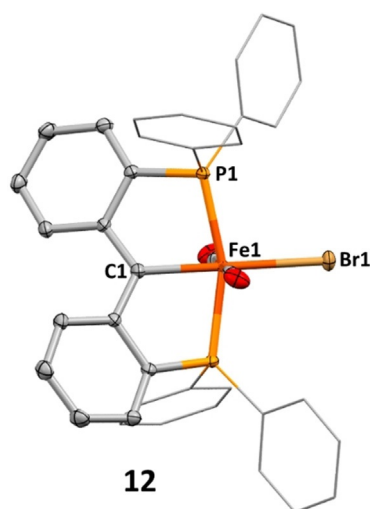


Figure 7. Molecular structure of compound **12**. Hydrogen atoms omitted, thermal ellipsoids shown at 50%. Selected bond distances (Å) and angles (°): Fe1-P1, 2.236(1); Fe1-C1, 1.998(2); Fe1-Br1, 2.487(1); P1-Fe1-P2, 161.3(1); C1-Fe1-Br1, 180.0(1).

Solid-state FTIR of the isolated product found new CO stretching bands at 1826 cm^{-1} and 1767 cm^{-1} indicative of a significantly reduced iron centre. Solid-state EPR spectroscopic analysis of the solid microcrystalline product revealed a signal at $g_{\text{iso}} = 2.005$, confirming the formation of a carbon-based radical species.

Compound **K[13]** was found to be extremely reactive, and readily underwent hydrogen atom abstraction with a number of solvents to form the $\text{PC}_{\text{alkyl}}\text{P}$ ferrate **K[14]** (Scheme 6B). For example, dissolution of **K[13]** in dry THF led to an initially purple solution that quickly (< 1 min) turned brown with the formation of **K[14]** in 43% ^{31}P NMR yield. Similarly, **K[13]** activated C–H bonds in MeCN, 9,10-dihydroanthracene (DHA) and NEt_3 . Reaction with MeCN-d_3 generated the isotopologue **K[14-d]** confirming the solvent as the hydrogen source, with deuterium present on the pincer alkyl position, as confirmed by ^2H NMR. Due to this reactivity and its poor solubility in arene solvents, solution characterization of **K[13]** could not be conducted, although the constitution of **K[13]** is verified through characterization of its hydrogen atom transfer (HAT) product **K[14]** and by in silico studies (see below).

Addition of 1,4,7,10,13,16-hexaoxacyclooctadecane (18-crown-6 ether) to a solution of **K[14]** allowed the formation of crystals of **[K(18-crown-6)][14]**, which were isolated in 25% yield and crystallographically characterized. The structure of **[K(18-crown-6)][14]** (Figure 8) confirmed that the $\text{PC}_{\text{carbene}}\text{P}$ ligand had been transformed into a $\text{PC}_{\text{alkyl}}\text{P}$ pincer ligand through HAT to the carbene position of **K[13]**. A relatively large Fe–C distance of $2.160(2)\text{ Å}$ to the alkyl ligand was observed. Additionally, the C–O distances in both carbonyl ligands were elongated at $1.175(3)\text{ Å}$ and $1.174(3)\text{ Å}$, signifying significant retrodonation from the metal centre. Finally, the potassium counter cation that had been captured by the crown ether was also supported by connection to a carbonyl oxygen position {O1–K1 = $2.803(2)\text{ Å}$ }.

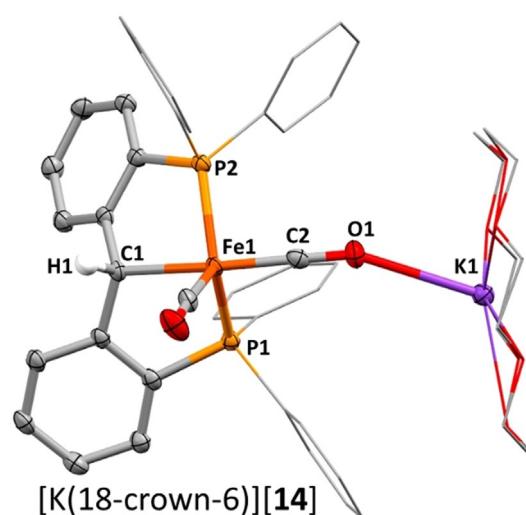


Figure 8. Molecular structure of compound **[K(18-crown-6)][14]**. Hydrogen atoms omitted (except H1), thermal ellipsoids shown at 50%. Selected bond distances (Å) and angles (°): Fe1-P1, 2.140(1); Fe1-C1, 2.160(2); C2-O1, 1.175(2); O1-K1, 2.803(2); P1-Fe1-P2, 126.5(1); C1-Fe1-C2, 165.8(1).

^1H NMR spectroscopic data for **K[14]** confirmed the transfer of a hydrogen atom to the carbene position with a signal at $\delta_{\text{H}} = 5.51$ (t, $^3J_{\text{PH}} = 4.8\text{ Hz}$) indicative of an α -alkyl hydrogen in the $\text{PC}_{\text{alkyl}}\text{P}$ ligand. ^{31}P NMR data revealed a single NMR environment for phosphorus with a signal at $\delta_{\text{P}} = 81.7$. IR CO stretching frequencies at 1864 cm^{-1} and 1804 cm^{-1} confirmed significant retrodonation to the carbonyl ligands, as observed in the solid-state structure.

DFT Studies

Further insight to the electronic structure of the $\text{PC}_{\text{carbene}}\text{P}$ complexes **1**, **[11-X]⁺** (X = Br, I), **12** and **[13][−]** was gained from DFT analysis. As stated above, geometry optimization (BP86SDD/6-31G**) of **1** showed a square pyramidal geometry to be slightly lower in energy than a trigonal bipyramidal structure. In fact, the latter corresponds to a transition state ($\Delta G^\ddagger = 5.2\text{ kcal mol}^{-1}$, $\nu_{\text{TS}} = i18\text{ cm}^{-1}$) in a shallow region of the potential energy surface that connects between square pyramidal minima, indicating that the crystal matrix is critical for stabilizing **1-TBP** within its unit cell. The optimized structures of **[11-X]⁺** (X = Br, I) and **12** are octahedral, as expected from their X-ray crystal structures, while the optimized structure of **[13][−]** is pseudo square pyramidal.

Calculated Frontier Kohn–Sham molecular orbitals of **1** show the HOMO to be largely located on the metal–carbene linkage (15% occupancy on the carbenic atom, 43% on Fe, Table 1). This renders the carbon relatively nucleophilic. In comparison, the calculated HOMO contribution on the carbenic carbon of the isoelectronic complex $[\text{PC}_{\text{carbene}}\text{PCo}(\text{PMe}_3)_2]^+$ (Figure 1, **II**) is only 7%, with 61% of the HOMO located on the cobalt centre of **II** (see SI, Figure S56).

The HOMO of compound **[11-Br]⁺** reveals that this MO has a negligible contribution from the carbenic position (0.6%, Table 1) and resides predominantly on the bromo

Table 1: Calculated molecular orbital parameters for PC_{carbene}P pincer complexes **1**, [11-X]⁺ (X = Br, I), **12** and [13]⁻.

	$f^{(2)}(\text{C})$	$f^{(2)}(\text{Fe})$	% HOMO		% LUMO	
			C	Fe	C	Fe
1	-0.01	-0.03	15.1	43.0	17.2	29.4
[11-Br] ⁺	0.09	-0.07	0.6	35.6	31.0	15.8
[11-I] ⁺	0.09	-0.06	0.4	24.1	31.3	15.1
12	-0.06	-0.02	31.3	13.0	28.6	10.1
[13] ⁻	-0.05	0.02	20.6	22.4	14.9	22.8

$f^{(2)}$ is Fukui descriptor (B3LYP/SDD/6-31G**) giving preferable site for nucleophilic attack (>0) or electrophilic attack (<0).

ligand (52%, see SI, Figure S58) and the iron centre (36%, Table 1). The HOMO of compound [11-I]⁺ is even more polarized towards the halide ligand, as would be expected from its higher π -donor ability. The iodo position supports 76% of the HOMO (see SI, Figure S59) and the carbene position accounts for only 0.4% of the HOMO (Table 1). Thus, the carbene positions in [11-X]⁺ (X = Br, I) are not nucleophilic, however, the LUMOs of [11-X]⁺ (X = Br, I) are dominated by the carbene carbon atom (C_{carbene} LUMO contribution: 31% for [11-Br]⁺, 31% for [11-I]⁺, Table 1), rendering this position relatively electrophilic in both complexes.

Interestingly, in the case of **12** both the HOMO (SOMO) and LUMO are predominantly localised on the carbenic position. This supports the assignment of **12** as a radical carbene, rather than a formally iron(I) 19-electron complex. Indeed, PC_{carbene}P type ligands have been shown to support radical carbene character on group 10 metals.^[9] The calculated spin density for **12** also corroborates a high degree of delocalization throughout the pincer diphenylene backbone with a total α -spin population of 0.9 e⁻ (0.5 e⁻ located on carbenic centre), providing added stability to the radical carbene (Figure 7). Likewise, the calculated HOMO and LUMO for [13]⁻ are also supported through delocalization

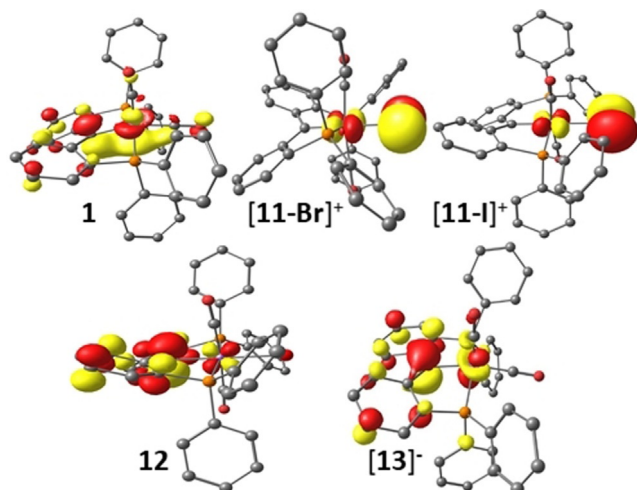


Figure 9. Calculated HOMOs for **1** (top left), [11-Br]⁺ (top centre), [11-I]⁺ (top right), **12** (bottom left) and [13]⁻ (bottom right). The SOMOs of **12** and [13]⁻ have a high degree of delocalization through their phenylene pincer systems indicative of radical carbene character.

onto the PC_{carbene}P ligand (Figure 9), with 20.6% of the HOMO and 14.9% of the LUMO residing on the carbene carbon. However, the iron centre still dominates both orbitals, contributing 22.4% to the LUMO and 22.8% to the HOMO (Table 1). Taken together with an α -spin population of 0.39 e⁻ on the iron centre in [13]⁻ versus 0.11 e⁻ on Fe in **12** (see SI, Figures S60–61), this is consistent with a notably reduced iron centre that lies along the spectrum between a formal Fe⁻¹ centre and a carbene supported radical.

Another measure of relative electrophilicity and nucleophilicity, the Fukui parameter, supports the above FMO analysis. Calculated Fukui parameters (B3LYP/SDD/6-31G**) assign both the carbene and iron centre as nucleophilic in **1**. This is supported by protonation of **1** to generate [10]⁺, and also by reaction of **1** with bromine and iodine to generate complexes [11-X]⁺ (X = Br, I), representing electrophilic attack at both the carbon and iron positions in **1**. In contrast, the Fukui parameters for compounds [11-X]⁺ (X = Br, I) denote the carbon as an electrophilic position. In the case of **12**, the Fukui parameters are diagnostic of a strongly nucleophilic carbene position, agreeing with the carbene radical assignment. Similarly, the one-electron reduced species [13]⁻ also reveals enhanced nucleophilicity at the carbene centre, while the iron is more electrophilic. It should be noted that the Fukui function only accounts for changes in the electron densities of the FMOs in response to changes of the total number of electrons, and does not take into account geometry, coordinative saturation or the nature of different electrophiles/nucleophiles (e.g. hard/soft classification). Although the iron centres in [11-X]⁺ (X = Br, I) and **12** are assigned as electrophilic, coordinative saturation of the iron positions precludes such reactivity in practice.

Conclusion

In summary, we have demonstrated facile access to an iron(0) PC_{carbene}P pincer system (**1**) via a ligand dehydration approach. Compound **1** is formed via an α -hydroxyalkyl hydride intermediate (**3**), that eliminates water under basic conditions to generate **1**. The carbene donor is found to facilitate the migration of a carbonyl ligand to the Fe-C carbene linkage generating a ketene species, thus allowing the Fe⁰ centre to accept an additional L type ligand (compounds **5** and **6**).

In agreement with prior reports on the PC_{carbene}P pincer ligand system, **1** is able to activate H-E (E = H, B, Cl) bonds via formal 1,2-addition across the alkylidene linkage to generate compounds **7–9**. However, in contrast to other examples, activation proceeds via carbonyl sequestration by the pincer ligand to facilitate coordination of the substrate (H₂ or HBpin) as opposed to direct concerted addition across the carbene. In the case of compound **8**, the activated components of H-Bpin could be further transferred to benzaldehyde to form BnOBpin and regenerate **1**, constituting a formal catalytic cycle that utilizes ligand cooperative activation.

Lastly, the ability of the PC_{carbene}P pincer ligand to support a number of oxidation states is demonstrated via a two

electron oxidation to form compounds $[\mathbf{11-X}][\text{BAR}^{\text{F}}_{20}]$ ($X = \text{Br, I}$), a one electron oxidation to generate $\mathbf{12}$, and a one electron reduction to form $\text{K}[\mathbf{13}]$. Compounds $[\mathbf{11-X}][\text{BAR}^{\text{F}}_{20}]$ ($X = \text{Br, I}$), $\mathbf{12}$ and $\text{K}[\mathbf{13}]$ can be viewed as having formal oxidation states of Fe^{II} , Fe^{I} and $\text{Fe}^{-\text{I}}$ respectively, but DFT analysis suggests that $\mathbf{12}$ and $\text{K}[\mathbf{13}]$ have much of their SOMO localised on the $\text{PC}_{\text{carbene}}\text{P}$ pincer framework, so are best described as radical carbenes. The utility of radical carbenes supported by iron is demonstrated through C-H activation in a range of inert small molecules.

Acknowledgements

We thank the Singapore Ministry of Education (WBS R-143-000-A05-112) and the Singapore Agency for Science, Technology and Research (A*STAR grant No. A1983c0033) for financial support. The authors wish to acknowledge the Irish Centre for High-End Computing (ICHEC) for the provision of computational facilities and support.

Conflict of Interest

The authors declare no conflict of interest.

Stichwörter: bond activation · carbene ligands · iron · pincer ligands · radicals

- [1] a) G. van Koten, D. Milstein, *Organometallic Pincer Chemistry; Topics in Organometallic Chemistry, Vol. 40*, Springer, Berlin, **2013**; b) G. van Koten, R. A. Gossage, *The Privileged Pincer-Metal Platform: Coordination Chemistry & Applications*, Springer, Berlin, **2015**.
- [2] a) C. J. Moulton, B. L. Shaw, *J. Chem. Soc. Dalton Trans.* **1976**, 1020; b) H. D. Empsall, E. M. Hyde, R. Markham, W. S. McDonald, M. C. Norton, B. L. Shaw, B. Weeks, *J. Chem. Soc. Chem. Commun.* **1977**, 589.
- [3] a) P. Chirik, R. Morris, *Acc. Chem. Res.* **2015**, *48*, 2495; b) I. Bauer, H.-J. Knölker, *Chem. Rev.* **2015**, *115*, 3170; c) C. Bolm, *Nat. Chem.* **2009**, *1*, 420; d) P. T. Anastas, J. C. Warner, *Green Chemistry: Theory and Practice*, Oxford University Press, Oxford, **1998**.
- [4] J. R. Khusnutdinova, D. Milstein, *Angew. Chem. Int. Ed.* **2015**, *54*, 12236; *Angew. Chem.* **2015**, *127*, 12406.
- [5] K.-S. Feichtner, V. H. Gessner, *Chem. Commun.* **2018**, *54*, 6540.
- [6] a) D. V. Gutsulyak, W. E. Piers, J. Borau-Garcia, M. Parvez, *J. Am. Chem. Soc.* **2013**, *135*, 11776; b) C. C. Comanescu, V. M. Iluc, *Polyhedron* **2018**, *143*, 176; c) C. C. Comanescu, V. M. Iluc, *Chem. Commun.* **2016**, *52*, 9048; d) E. A. LaPierre, W. E. Piers, C. Gendy, *Dalton Trans.* **2018**, *47*, 16789; e) J. D. Smith, G. Durrant, D. H. Ess, B. S. Gelfand, W. E. Piers, *Chem. Sci.* **2020**, *11*, 10705.
- [7] a) S. Sung, Q. Wang, T. Krämer, R. D. Young, *Chem. Sci.* **2018**, *9*, 8234; b) S. Sung, T. Joachim, T. Krämer, R. D. Young, *Organometallics* **2017**, *36*, 3117; c) Q. Wang, H. Tinnermann, S. Tan, R. D. Young, *Organometallics* **2019**, *38*, 3512; d) E. A. LaPierre, W. E. Piers, C. Gendy, *Organometallics* **2018**, *37*, 3394.
- [8] P. Cui, C. C. Comanescu, V. M. Iluc, *Chem. Commun.* **2015**, *51*, 6206.
- [9] a) C. C. Comanescu, M. Vyushkova, V. M. Iluc, *Chem. Sci.* **2015**, *6*, 4570; b) P. Cui, V. M. Iluc, *Chem. Sci.* **2015**, *6*, 7343; c) P. Cui, M. R. Hoffbauer, M. Vyushkova, V. M. Iluc, *Chem. Sci.* **2016**, *7*, 4444; d) P. Cui, M. R. Hoffbauer, M. Vyushkova, V. M. Iluc, *Dalton Trans.* **2019**, *48*, 9663; e) A. P. Deziel, M. R. Hoffbauer, V. M. Iluc, *Organometallics* **2019**, *38*, 879; f) R. J. Burford, W. E. Piers, M. Parvez, *Eur. J. Inorg. Chem.* **2013**, 3826.
- [10] a) L. E. Doyle, W. E. Piers, J. Borau-Garcia, *J. Am. Chem. Soc.* **2015**, *137*, 2187; b) L. E. Doyle, W. E. Piers, J. Borau-Garcia, M. J. Sgro, D. M. Spasyuk, *Chem. Sci.* **2016**, *7*, 921; c) L. E. Doyle, W. E. Piers, D. W. Bia, *Dalton Trans.* **2017**, *46*, 4346; d) J. D. Smith, E. Chih, W. E. Piers, D. M. Spasyuk, *Polyhedron* **2018**, *155*, 281; e) P. E. Rothstein, C. C. Comanescu, V. M. Iluc, *Chem. Eur. J.* **2017**, *23*, 16948; f) H. Tinnermann, S. Sung, B. A. Cala, H. J. Gill, R. D. Young, *Organometallics* **2020**, *39*, 797; g) H. Tinnermann, R. D. Young, *Chem. Asian J.* **2020**, *15*, 2873.
- [11] S. Sung, R. D. Young, *Dalton Trans.* **2017**, *46*, 15407.
- [12] a) W. Weng, S. Parkin, O. V. Ozerov, *Organometallics* **2006**, *25*, 5345; b) R. J. Burford, W. E. Piers, D. H. Ess, M. Parvez, *J. Am. Chem. Soc.* **2014**, *136*, 3256.
- [13] a) D. G. Gusev, A. J. Lough, *Organometallics* **2002**, *21*, 2601; b) R. J. Burford, W. E. Piers, M. Parvez, *Organometallics* **2012**, *31*, 2949; c) E. A. LaPierre, W. E. Piers, J.-B. Lin, C. Gendy, *Chem. Eur. J.* **2019**, *25*, 4305; d) A. V. Polukeev, O. F. Wendt, *J. Organomet. Chem.* **2018**, *867*, 33; e) A. V. Polukeev, O. F. Wendt, *Organometallics* **2017**, *36*, 639; f) J. R. Logan, W. E. Piers, J. Borau-Garcia, D. M. Spasyuk, *Organometallics* **2016**, *35*, 1279.
- [14] An iron $\text{PC}_{\text{carbene}}\text{P}$ complex obtained via double deprotonation of a methylene proligand was reported by Iluc during the revision of this manuscript, see: M. R. Hoffbauer, V. M. Iluc, *J. Am. Chem. Soc.* **2021**, *143*, 5592.
- [15] S. Sung, H. Tinnermann, T. Krämer, R. D. Young, *Dalton Trans.* **2019**, *48*, 9920.
- [16] A. Dauth, U. Gellrich, Y. Diskin-Posner, Y. Ben-David, D. Milstein, *J. Am. Chem. Soc.* **2017**, *139*, 2799.
- [17] S. Garhwal, A. Kaushansky, N. Fridman, L. J. W. Shimon, G. de Ruiter, *J. Am. Chem. Soc.* **2020**, *142*, 17131.
- [18] For examples see: a) A. Shojaja, J. D. Atwood, *Organometallics* **1985**, *4*, 187; b) J. Shen, Y. Shi, Y. Gao, Q. Shi, F. Basolo, *J. Am. Chem. Soc.* **1988**, *110*, 2414; c) B. F. G. Johnson, Y. V. Roberts, *J. Cluster Sci.* **1993**, *4*, 231; d) J. D. Atwood, *J. Organomet. Chem.* **1990**, *383*, 59.
- [19] B. Cordero, V. Gómez, A. E. Platero-Prats, M. Revés, J. Echeverría, E. Cremades, F. Barragán, S. Alvarez, *Dalton Trans.* **2008**, 2832.
- [20] a) M. Brookhart, W. A. Chandler, A. C. Pfister, C. C. Santlani, P. S. White, *Organometallics* **1992**, *11*, 1263; b) S. D. Ittel, C. A. Tolman, P. J. Krusic, A. D. English, J. P. Jesson, *Inorg. Chem.* **1978**, *17*, 3432.
- [21] Single C-H activation of related methylene linked pincer proligands using Fe^0 is known, but double C-H activation has not been reported, see: H. Zhao, H. Sun, X. Li, *Organometallics* **2014**, *33*, 3535.
- [22] S. Sung, J. K. Boon, J. J. C. Lee, N. A. Rajabi, S. A. Macgregor, T. Krämer, R. D. Young, *Organometallics* **2017**, *36*, 1609.
- [23] A. W. Addison, T. N. Rao, J. Reedijk, J. van Rijn, G. C. Verschoor, *J. Chem. Soc. Dalton Trans.* **1984**, 1349. Note: Calculated τ values determine **1-TBP** to be a borderline case between SQP and TBP geometries, but is assigned TBP due to its crystallographically imposed C_2 symmetry and higher degree of TBP character as compared to **1-SQP**.
- [24] a) R. J. Trovitch, E. Lobkovsky, P. J. Chirik, *Inorg. Chem.* **2006**, *45*, 7252; b) E. M. Pelczar, T. J. Emge, K. Krogh-Jespersen, A. S. Goldman, *Organometallics* **2008**, *27*, 5759.
- [25] J. D. Smith, J. R. Logan, L. E. Doyle, R. J. Burford, S. Sugawara, C. Ohnita, Y. Yamamoto, W. E. Piers, D. M. Spasyuk, J. Borau-Garcia, *Dalton Trans.* **2016**, *45*, 12669.
- [26] a) B. M. Lindley, B. P. Jacobs, S. N. MacMillan, P. T. Wolczanski, *Chem. Commun.* **2016**, *52*, 3891; b) C. H. Arnett, T. Agapie, J.

- Am. Chem. Soc.* **2020**, *142*, 10059; c) B. M. Lindley, A. Swidan, E. B. Lobkovsky, P. T. Wolczanski, M. Adelhardt, J. Sutter, K. Meyer, *Chem. Sci.* **2015**, *6*, 4730.
- [27] J. Weismann, R. Waterman, V. H. Gessner, *Chem. Eur. J.* **2016**, *22*, 3846.
- [28] S. K. Russell, J. M. Hoyt, S. C. Bart, C. Milsman, S. C. E. Stieber, S. P. Semproni, S. DeBeer, P. J. Chirik, *Chem. Sci.* **2014**, *5*, 1168.

Manuskript erhalten: 2. April 2021
Veränderte Fassung erhalten: 17. Juni 2021
Akzeptierte Fassung online: 18. Juni 2021
Endgültige Fassung online: 9. Juli 2021
